International Journal of Thermophysics, Vol. 24, No. 4, July 2003 (© 2003)

A Rational Helmholtz Fundamental Equation of State for Difluoromethane with an Intermolecular Potential Background

I M. Astina[1] **and H. Sato**[1,2]

Received February 3, 2003

A new fundamental thermodynamic equation of state for difluoromethane was developed by considering the intermolecular potential behavior for improving the reliability in the gaseous phase. Reliable second and third virial coefficients are introduced in accordance with the principle of a unified relation of the intermolecular potential energy and the fundamental equation of state. The fundamental equation of state is able to provide reliable thermodynamic properties even at low temperatures or in the region near saturation where precise and accurate experimental data are not available. The estimated uncertainties of calculated properties from the equation of state are 0.07% in density for the liquid phase, 0.1% in pressure for the gaseous phase, 0.35% in pressure for the supercritical region, 0.07% in vapor pressure, 0.2% in saturated-liquid density, 0.7% in saturated-vapor density, 0.01% in speed of sound for the gaseous phase, 0.7% in speed of sound for the liquid phase, and 0.6% in isochoric specific heat for the liquid phase. The equation is valid for temperatures from the triple point to 450 K and pressures up to 72 MPa.

KEY WORDS: difluoromethane; equation of state; HFC-32; HFC refrigerant; intermolecular potential; R32.

1. INTRODUCTION

Difluoromethane (R32) is an alternative refrigerant, which has been proposed as a component of mixtures blending with other refrigerants such as R134a, R125, R152a, or R143a, to replace R22. Several existing equations

[1] Center for Space and Environmental Design, School of Science for Open and Environmental Systems, Graduate School of Science and Technology, Keio University, 3-14-1 Hiyoshi, Kohoku-ku, Yokohama 223-8522, Japan.

[2] To whom correspondence should be addressed. E-mail: hsato@sd.keio.ac.jp

0195-928X/03/0700-0963/0 © 2003 Plenum Publishing Corporation

of state (EOS) are available including the MBWR-type EOS by Outcalt and McLinden [1], the Helmholtz-type EOS by Tillner-Roth and Yokozeki [2], and an equation by Vassermann and Fominsky [3]. Moreover, the International Energy Agency-Annex 18 has recommended the Helmholtz-type EOS developed by Tillner-Roth and Yokozeki as an International Standard equation of state for R32. Nevertheless, our recent investigation and assessment of the existing EOS indicated several improper behaviors in the EOS. The EOS by Tillner-Roth and Yokozeki represents the available experimental data well, but improper behaviors still remain when the thermodynamic properties are calculated from the EOS. They happen in the gaseous phase at low temperatures where the measurements for both caloric and $p\rho T$ properties are very scarce as shown in Fig. 1, as well as in the gaseous phase very near saturation. The improper behaviors indicate that assessments based only on the deviation of calculated property values from experimental data are not sufficiently adequate to verify the reliability of the EOS. Theoretical assessments should be involved in order to obtain consistent relations among the calculated property values and to obey the universal laws of thermodynamics.

Narukawa et al. [4] from our group studied the thermodynamic consistency among the thermodynamic properties of hydrofluorocarbon (HFC) refrigerants in the gaseous phase at low temperatures and near saturation. They pointed out that there is a large difference (5% in the worst case) among specific heat values in the gaseous phase near saturation derived from different existing Helmholtz EOS, including internationally recommended EOS for R32. Matsuda et al. [5] from our group also

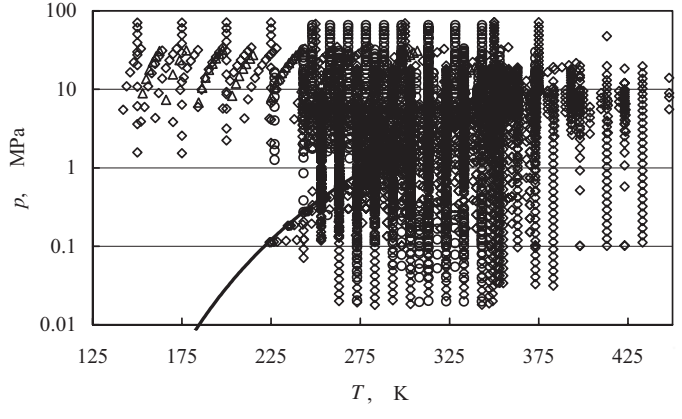

Fig. 1. Existing experimental data for R32. (△) c_p; (○) c_v; (◇) $p\rho T$; (□) w.

simultaneously reported a similar result for R32 based on their experimental work, which involved accurate and precise measurements of $p\rho T$ in the liquid and gaseous phases, including the region very near saturation. Due to the importance in air conditioning and refrigeration applications, improvements of the existing EOS are needed.

Reliable input data at any state point over the covered ranges are needed in modeling a wide thermodynamic surface. This may not always be satisfied experimentally. An alternative way to develop a reliable EOS would be not only to base it on experimental data but also to use theoretical background information such as virial coefficients derived from the intermolecular potential energy. This alternative method will be introduced in this report, and a comprehensive analysis of the mathematical and modeling aspects will be provided.

2. DEVELOPMENT OF AN EQUATION OF STATE WITH AN INTERMOLECULAR POTENTIAL MODEL BACKGROUND

The importance of considering a virial EOS to develop a fundamental Helmholtz EOS lies in its rigorous theoretical foundation by which virial coefficients appear not only as empirical constants but also as a representation of the intermolecular potential energy. The virial coefficients are related analytically to the intermolecular potential energy of clusters of molecules. The second virial coefficient arises from the interaction between a pair of molecules, the third virial coefficient depends on the interaction of clusters of three molecules, etc.

As a fundamental model of the thermodynamic properties for a fluid, an EOS should be able to represent not only measurements of thermodynamic properties but also the properties in regions where no experimental data are available. The properties should be reasonably represented according to theoretical background behavior of the gaseous, liquid, supercritical, and saturation states. A statistical thermodynamic analysis for forces between molecules has already shown the exact relation of virial coefficients and the intermolecular potential energy. Therefore, no rational reason can be accepted if the EOS cannot reliably derive the virial coefficients.

In addition, the shortage and inconsistency of thermodynamic relationships among experimental data cause inaccurate EOS. Theoretical background results can be used to improve the reliability of an EOS at low temperatures, especially in the region near saturation. Several intermolecular potential models such as the hard-sphere potential, the Kihara potential, the Lennard-Jones potential, the square-well potential, the Stockmayer potential, etc., can be considered when developing an EOS.

The optimum selection of a model for a specified fluid will help reveal its proper behavior.

In practice, virial coefficients were derived from intermolecular potential models and empirically determined by fitting to experimental data. The intermolecular potential model can be determined from speed-of-sound measurements with or without $p\rho T$ measurements. Gillis and Moldover [6] discussed in detail how the hard-core-square-well potential could be used to obtain the virial EOS from speed-of-sound data. Concerning HFC refrigerants, Yokozeki et al. [7] from our group examined and deduced the virial coefficients with the Stockmayer potential. Gillis [8] also reported a set of molecular constants from the hard-core-square-well potential for HFC refrigerants, which was derived from speed-of-sound data. These efforts were focused on finding a new potential model for representing thermophysical properties with very high accuracy. In 2002, Kojima and Sato [9] from our group proposed a practical modification parameter to improve the representation of the square-well and Stockmayer potential models. This modification made it possible to predict the thermodynamic properties in the gaseous phase based only on a limited number of speed-of-sound measurements, and the potential models can be applied without any change but with the new temperature parameter.

Additional work using different approaches to obtain virial coefficients were also reported by other members of our group. Considering reliable experimental data for both gaseous speed-of-sound and $p\rho T$ properties, an empirical function form of the virial coefficients was proposed by Zhang et al. [10]. Narukawa et al. [4] examined the existing EOS for several HFC refrigerants, and proposed a virial EOS with the third virial coefficients derived by Yokozeki et al. based on the Stockmayer potential model and the second virial coefficients fit to experimental data. Matsuda et al. [5] reported another framework by fitting the virial EOS to newly obtained accurate $p\rho T$ measurements with a magnetic suspension densimeter especially near saturation. They assessed the existing EOS using their measurements and proposed a highly accurate virial EOS that can represent densities especially in the gaseous phase near saturation with high accuracy.

As one of a series of efforts in our group concerning theoretical and empirical approaches, a fundamental EOS explicitly represented in the Helmholtz free energy function was established in this study. The second and third virial coefficients were checked carefully in the process of modeling by adjusting the primary and secondary differentiations of the free energy function. Reasonable mathematical and physical background behavior was also confirmed for determination of the third virial coefficient. It is important to reduce the degrees of freedom of the free energy

function. From relations of the thermodynamic properties from the free energy function listed in Section 6, it can be seen that secondary differentiation of the free energy function with respect to reduced density is contained in relations of the third virial coefficient, speed of sound, and isobaric specific heat. Not only the speed of sound and isobaric specific heat, but also the third virial coefficient with a background of the intermolecular potential energy should be considered in the modeling.

The optimization method for selecting terms of EOS was originally developed in accordance with a genetic algorithm that is one of several categories included in evolutionary computation [11]. Object-oriented programming language C++ was applied for the optimization. In the optimization process, three operators, i.e., recombination, mutation, and selection were introduced. Recombination is a marriage process of two individuals to reproduce offspring, mutation is a representation of duplicate error inherited to offspring, and selection is a process to find the best individual when offspring survive with other individuals until a following process of determination of parents to reproduce the next generation. A detailed explanation of the optimization method will be presented in another paper [12].

3. INPUT PARAMETERS AND INPUT DATA

All thermodynamic properties for the ideal gas, compressed liquid, superheated vapor, supercritical fluid, and saturation of a fluid can be derived from the Helmholtz free energy function. The Helmholtz EOS should be established by involving the free energy function and its differentiations for exactly representing each thermodynamic property. Indeed, the Helmholtz EOS implicitly uses the ideal-gas correlation, but the real gas at low temperatures is not satisfactorily represented in the most cases. From efforts to improve representation of the Helmholtz EOS regarding the behavior of the second and third virial coefficients, the specific heat properties in the gaseous phase at low temperatures were possibly determined. Virial coefficients from an intermolecular potential background were involved in the regression of this study, while experimental data were always used as primary input data. This process enables the development of an EOS that can represent the thermodynamic properties accurately even at very low temperatures where no experimental data are available.

A survey of thermophysical property data for R32 was reported by Šifner et al. [13]. Several experimental data such as Kunimoto et al. [14] and Kubota et al. [15] were not included in Šifner's report. Several new

data such as speed-of-sound measurements by Pires and Guedes [16] and $p\rho T$ measurements by Matsuda et al. [5] were reported later.

A new EOS was established by considering data for $p\rho T$, caloric properties, and virial coefficients. Two groups of input data are involved in modeling: derived data and experimental data. The derived data include $p\rho T$ at saturation, virial coefficients, and isochoric specific heat. Derived data for $p\rho T$ at saturation are needed because of the difficulty to obtain reliable data at the same temperatures from the triple point to critical point. Derived data for isochoric specific heat are introduced for the gaseous phase especially near saturation, and virial coefficient data cover temperatures from the triple point to the upper limit of temperature. Further information for the derived data is given in Section 4.

Assessment of experimental data was performed to find a reliable set for modeling. Experimental $p\rho T$ data for the superheated vapor were chosen from 408 points of de Vries [17] and 144 points of Matsuda et al. [5]. For the compressed liquid, 408 points of de Vries [17], 120 points of Magee [18], and 75 points of Matsuda et al. [5] were chosen. Additionally, 43 points of Holste et al. [19] at higher pressures than 25 MPa were chosen in order to compensate the limited data at higher pressures. Data for the supercritical states were chosen from 240 points of de Vries [17] (by means of Burnet and vibrating tube measurements), 14 points of Magee [18], and 9 points of Holste et al. [19] at pressures higher than 25 MPa. Based on a consistency assessment for the data of Holste et al. [19] against the data of Magee and of de Vries, density values of Holste et al. [19] were adjusted by $+0.15\%$ to obtain consistent results with other data. All of the basic data for the isochoric specific heat in the liquid phase by Lüddecke and Magee [20] were selected as input data. Data for the speed of sound included 111 points of Takagi [21], 304 points of Pires and Guedes [16], and 30 points of Grebenkov et al. [22] for the liquid phase, and 67 points of Hozumi et al. [23] for the gaseous phase.

4. IMPORTANT PARAMETERS AND ANCILLARY EQUATIONS

Several important parameters are needed to develop and implement both the fundamental EOS and the ancillary equations for R32. They consist of the critical point, triple point, gas constant, and molar mass. The selected critical temperature is 351.255 K [24], and the critical density is 424 $kg \cdot m^{-3}$ [24]. The critical pressure, which was obtained from extrapolating a developed vapor pressure equation in this study, is 5.780 MPa. These critical values are the same as the values recommended by JARef [25]. The triple point is 136.34 K [18], which is the lower limit of a new

EOS. The universal gas constant is 8.314472 $J \cdot mol^{-1} \cdot K^{-1}$ [26], and the molar mass is 0.052023 $kg \cdot mol^{-1}$.

Ancillary equations were used to calculate the virial coefficients, the specific heat in the gaseous phase, and $p\rho T$ at saturation. The virial coefficients considered in this study were deduced from Narukawa et al. [4] and Matsuda et al. [5]. Both studies have a common correlation expressed as

$$Z = \frac{p}{\rho RT} = 1 + B(T_r)\,\rho + C(T_r)\,\rho^2 \tag{1}$$

The second and third virial coefficients are given as

$$B(T_r) = b_1 + b_2 T_r^{-1} + b_3 \exp(b_4 T_r^{-1}) \tag{2}$$

$$C(T_r) = c_1 + c_2 T_r^{-\alpha} + c_3 T_r^{-\beta} \tag{3}$$

where $T_r = T/T_c$. Numerical parameters for the virial coefficients are given in Table I.

Virial coefficients developed by Narukawa et al. [4] (with a reanalysis for the results of Yokozeki et al. [7] by adjusting for caloric and experimental $p\rho T$ data at low densities in the gaseous phase) were used to generate input data for the second and third virial coefficients. Virial coefficients developed by Matsuda et al. [5] can more accurately represent caloric and $p\rho T$ properties in the gaseous phase for higher densities. By using the virial EOS by Matsuda et al. and the equation for the ideal-gas specific heat established in this work, specific heat values in the gaseous phase at pressures lower than 2 MPa were used to prepare the input data.

Three ancillary equations for calculating vapor pressure, saturated-vapor density, and saturated-liquid density were developed to obtain good

Table I. Numerical Parameters for Virial Coefficients (Eqs. (2) and (3))

	Narukawa et al. [4]	Matsuda et al. [5]
b_1	1.09100×10^{-1}	1.04770×10^{-1}
b_2	-1.04704×10^{-1}	-9.94901×10^{-2}
b_3	-2.63081×10^{-2}	-2.65089×10^{-2}
b_4	2.03104×10^{0}	2.02266×10^{0}
c_1	1.38239×10^{-3}	8.46694×10^{-4}
c_2	1.93226×10^{-2}	1.77947×10^{-2}
c_3	-1.55865×10^{-3}	-8.12886×10^{-4}
α	3.224×10^{0}	3.22394×10^{0}
β	9.77×10^{0}	9.76976×10^{0}

thermodynamic consistency in the phase transition region from single-phase to two-phase states between the triple point and the critical point where they should be represented reliably. An equation for vapor pressures was expressed as

$$\ln \frac{p_s}{p_c} = \frac{T_c}{T} \sum_{i=1}^{4} c_i \left(1 - \frac{T}{T_c}\right)^{t_i} \tag{4}$$

where $c_1 = -7.439127$, $t_1 = 1$, $c_2 = 1.663651$, $t_2 = 1.5$, $c_3 = -1.889549$, $t_3 = 2.5$, $c_4 = -2.683971$, and $t_4 = 5$. Another ancillary equation is given for calculating saturated-liquid densities as

$$\frac{\rho'}{\rho_c} - 1 = \sum_{i=1}^{5} c_i \left(1 - \frac{T}{T_c}\right)^{t_i} \tag{5}$$

where $c_1 = 2.212008$, $t_1 = 1/3$, $c_2 = -1.919298$, $t_2 = 2/3$, $c_3 = 8.347534$, $t_3 = 1$, $c_4 = -10.466628$, $t_4 = 4/3$, $c_5 = 5.002808$, and $t_5 = 5/3$. The equation for calculating saturated-vapor densities is given as

$$\ln \left(\frac{\rho''}{\rho_c}\right) = \sum_{i=1}^{5} c_i \left(1 - \frac{T}{T_c}\right)^{t_i} \tag{6}$$

where $c_1 = -1.930810$, $t_1 = 1/3$, $c_2 = -2.168772$, $t_2 = 2/3$, $c_3 = -6.318893$, $t_3 = 4/3$, $c_4 = -20.341500$, $t_4 = 10/3$, $c_5 = -62.978835$, and $t_5 = 22/3$.

5. NEW FUNDAMENTAL EQUATION OF STATE

The new EOS is given as a Helmholtz free energy function. The function is given in dimensionless that was reduced by the gas constant and temperature, and divided into an ideal-gas part and a residual part. The ideal-gas part contains the properties of a fluid at the ideal-gas state. The residual part contains residual properties of the real fluid from the ideal-gas state of the fluid. The ideal-gas part was derived by means of integration of the ideal-gas specific heat equation, c_p°, and the residual part was established by multiproperty fitting for the selected experimental and derived data as explained in the previous section.

The equation for c_p° was established by fitting the calculated data of Yokozeki et al. [7], and optimized by selecting polynomial and Einstein–Planck terms. The selection was conducted according to the genetic

Table II. Coefficients and Parameters of the Ideal-Gas Part (Eq. (8))

i	N_i°	b_i°
0	$-8.253\,834 \times 10^0$	–
1	$6.351\,918 \times 10^0$	–
2	$2.999\,660 \times 10^0$	–
3	$3.121\,150 \times 10^0$	$4.559\,777 \times 10^0$
4	$9.994\,221 \times 10^{-1}$	$2.164\,788 \times 10^0$
5	$2.412\,721 \times 10^0$	$1.234\,687 \times 10^1$
6	$3.055\,435 \times 10^0$	$5.877\,902 \times 10^0$

optimization method. The equation, with numerical coefficients and parameters given in Table II, is expressed as

$$\frac{c_p^\circ}{R} = 1 + N_2^\circ + \sum_{i=3}^{6} N_i^\circ \tau^2 b_i^{\circ 2} \frac{\exp(-b_i^\circ \tau)}{\{1-\exp(-b_i^\circ \tau)\}^2} \tag{7}$$

The ideal-gas part was then derived by integration of c_p° with an integral boundary condition determined by fitting the EOS to a reference point of 200 $kJ \cdot kg^{-1}$ and 1 $kJ \cdot kg^{-1} \cdot K^{-1}$ for enthalpy and entropy values at the saturated-liquid state of 273.15 K. The ideal-gas part was expressed as

$$\alpha^\circ(\delta, \tau) = \ln \delta + N_0^\circ + N_1^\circ \tau + N_2^\circ \ln \tau + \sum_{i=3}^{6} N_i^\circ \ln\{1-\exp(-b_i^\circ \tau)\} \tag{8}$$

where N_0° and N_1° are the integration constants; and the numerical coefficients and parameters are given in Table II.

The residual part of the new EOS was optimized in accordance with a genetic optimization method, and the final result is written as

$$\alpha^r = \sum_{i=1}^{6} N_i\, \delta^{d_i} \tau^{t_i} + \sum_{i=7}^{11} N_i\, \delta^{d_i} \tau^{t_i} \exp(-\delta) + \sum_{i=12}^{15} N_i\, \delta^{d_i} \tau^{t_i} \exp(-\delta^2) + \sum_{i=16}^{18} N_i\, \delta^{d_i} \tau^{t_i} \exp(-\delta^3) \tag{9}$$

where the numerical coefficients and exponents are given in Table III.

Table III. Coefficients and Exponents of the Residual Part (Eq. (9))

i	N_i	d_i	t_i
1	2.118688×10^{0}	1	0.5
2	-4.531096×10^{0}	1	1.125
3	1.442456×10^{0}	1	1.625
4	2.053906×10^{-1}	3	0.875
5	-1.311675×10^{-1}	3	1.5
6	1.022272×10^{-2}	4	1.75
7	4.873982×10^{-1}	1	1.75
8	-1.062213×10^{0}	1	2.75
9	-4.542051×10^{-3}	5	0.25
10	-6.933347×10^{-4}	5	3.75
11	-3.510307×10^{-2}	6	1
12	-5.606161×10^{-2}	1	6.5
13	8.849625×10^{-2}	2	2.5
14	-1.850758×10^{-2}	5	7.5
15	7.878071×10^{-3}	6	7.5
16	-3.384115×10^{-2}	2	11
17	1.641979×10^{-4}	2	16
18	-1.459172×10^{-3}	8	13

6. THERMODYNAMIC PROPERTY RELATIONS FROM THE HELMHOLTZ FREE ENERGY

Relations of thermodynamic properties from the Helmholtz free energy can be derived from the basic laws of thermodynamics. The following equations are given for derivatives of thermodynamic properties with the Helmholtz free energy function as described in the previous section. The terms α^r_δ, $\alpha^r_{\delta\delta}$, α^r_τ, α°_τ, $\alpha^\circ_{\tau\tau}$, etc. represent the differentiations of α° or α^r with respect to either δ or τ, for example, $\alpha^r_{\delta\delta} = \partial^2\alpha^r/\partial\delta^2$.
Specific heat of ideal gas:

$$c_p^\circ(\tau)/R = 1 - \tau^2\alpha^\circ_{\tau\tau} = 1 + c_v^\circ(\tau)/R$$

Compressibility factor and pressure:

$$Z(\tau, \delta) = p(\tau, \delta)/(\rho RT) = 1 + \delta\alpha^r_\delta$$

Saturation property criteria:

$$p_s(\tau, \delta', \delta'')/(RT)(1/\rho'' - 1/\rho') - \ln(\delta'/\delta'') = \alpha^r(\tau, \delta') - \alpha^r(\tau, \delta'')$$

$$p_s(\tau, \delta')/(\rho' RT) = 1 + \delta'\alpha^r_{\delta'} \qquad p_s(\tau, \delta'')/(\rho'' RT) = 1 + \delta''\alpha^r_{\delta''}$$

Virial coefficients:

$$B(\tau)\,\rho_c = \lim_{\delta \to 0} \alpha^r_\delta \qquad C(\tau)\,\rho_c^2 = \lim_{\delta \to 0} \alpha^r_{\delta\delta}$$

Specific heat at constant volume:

$$c_v(\tau, \delta)/R = -\tau^2(\alpha^o_{\tau\tau} + \alpha^r_{\tau\tau})$$

Specific heat at constant pressure:

$$c_p(\tau, \delta)/R = -\tau^2(\alpha^o_{\tau\tau} + \alpha^r_{\tau\tau}) + \frac{(1 + \delta\alpha^r_\delta - \delta\tau\,\alpha^r_{\delta\tau})^2}{(1 + 2\,\delta\alpha^r_\delta + \delta^2\alpha^r_{\delta\delta})}$$

Saturated-liquid specific heat:

$$c'_s(\tau, \delta', \delta'')/R = \frac{c_v(\tau, \delta')}{R} + \frac{(1 + \delta'\alpha^{r'}_\delta - \delta'\tau\,\alpha^{r'}_{\delta\tau})}{(1 + 2\,\delta'\alpha^{r'}_\delta + \delta'^2\alpha^{r'}_{\delta\delta})} \times \left\{ 1 + \delta'\alpha^{r'}_\delta - \delta'\tau\,\alpha^{r'}_{\delta\tau} - \frac{1}{R\rho_c\delta'} \frac{dp_s(\tau, \delta', \delta'')}{dT} \right\}$$

Specific internal energy:

$$u(\tau, \delta)/(RT) = \tau(\alpha^o_\tau + \alpha^r_\tau)$$

Specific entropy:

$$s(\tau, \delta)/R = \tau(\alpha^o_\tau + \alpha^r_\tau) - (\alpha^o + \alpha^r)$$

Specific enthalpy:

$$h(\tau, \delta)/(RT) = \tau(\alpha^o_\tau + \alpha^r_\tau) + 1 + \delta\alpha^r_\delta$$

Speed of sound:

$$w(\tau, \delta)^2/(RT) = 1 + 2\,\delta\alpha^r_\delta + \delta^2\alpha^r_{\delta\delta} + \frac{(1 + \delta\alpha^r_\delta - \delta\tau\,\alpha^r_{\delta\tau})^2}{-\tau^2(\alpha^o_{\tau\tau} + \alpha^r_{\tau\tau})}$$

Specific Gibbs free energy:

$$g(\tau, \delta)/(RT) = 1 + \alpha^o + \alpha^r + \delta\alpha^r_\delta$$

Joule–Thomson coefficient:

$$\mu(\tau, \delta)\,R\rho = \frac{-(\delta\alpha^r_\delta + \delta^2\alpha^r_{\delta\delta} + \delta\tau\,\alpha^r_{\delta\tau})}{(1 + \delta\alpha^r_\delta - \delta\tau\,\alpha^r_{\delta\tau})^2 - \tau^2(\alpha^o_{\tau\tau} + \alpha^r_{\tau\tau})(1 + 2\,\delta\alpha^r_\delta + \delta^2\alpha^r_{\delta\delta})}$$

Fugacity:

$$f(\tau, \delta) = p \exp \{\alpha^r + \delta\alpha^r_\delta - \ln(1 + \delta\alpha^r_\delta)\}$$

7. RELIABILITY ASSESSMENTS

The ability of the new EOS to represent thermodynamic property values was assessed by comparisons with numerous sets of experimental data. The property values calculated from the EOS serve as a baseline for deviations. Statistical results of the comparisons are given in Tables IV to VI. Statistical definitions used for evaluation are as follows: AAD—average of absolute deviations; BIAS—average of deviations; STD—standard deviation; and Max. Dev.—the maximum of absolute

Table IV. Summary of Comparisons for Saturation Density Measurements

Source				AAD	BIAS	STD	Max. Dev.	
First Author	Ref.	Mtd[b]	N	(%)	(%)	(%)	(%)	N_{out}
				Saturated-liquid density				
Defibaugh[a]	28	4	21	0.095	0.079	0.14	0.47	–
Fukushima	29	5, 6, 7	21	0.44	0.070	0.60	1.4	1
Higashi	30	6	8	1.1	0.60	1.3	2.5	–
Holcomb	31	9	25	0.18	0.33	0.22	0.65	–
Kuwabara[a]	24	6	17	0.28	−0.42	0.33	0.98	–
Magee[a]	18	5	13	0.037	0.027	0.042	0.080	–
Malbrunot	32	1, 2	15	0.32	0.024	0.38	0.68	1
Sato	33	5	2	0.13	0.21	0.19	0.35	–
Shinsaka	34	7	19	0.079	−0.96	0.11	1.1	–
Widiatmo	35	3	22	0.067	−0.12	0.10	0.23	–
				Saturated-vapor density				
Defibaugh[a]	28	4	28	0.32	−0.03	0.36	0.61	–
Fukushima	29	5, 6, 7	13	1.3	−0.17	1.7	3.3	1
Higashi	30	6	9	1.4	2.3	2.0	5.1	–
Holcomb[a]	31	9	25	0.61	0.45	0.80	3.0	–
Kuwabara	24	6	13	0.81	−0.13	0.92	1.3	3
Sato	33	5	4	0.43	−1.41	0.51	1.9	–

[a] Selected in fitting the ancillary equations.

[b] Methods: (1) graphical extrapolation of isotherms to the vapor pressure curve, (2) pycnometric, (3) sinker with magnetic suspension, (4) isotherm extrapolation to the saturation boundary using the Tait equation, (5) intersection of isochores with vapor pressure curve, (6) meniscus disappearance, (7) pyrex-glass float, (8) vibrating-tube densimeter, (9) VLE-circulation apparatus.

Table V. Summary of Comparisons for Vapor Pressure Measurements

Source				AAD	BIAS	STD	Max. Dev.	
First Author	Ref.	Mtd[b]	N	(%)	(%)	(%)	(%)	N_{out}
Baroncini	36	7	56	0.086	0.015	0.10	0.25	–
Bouchot	37	9	8	0.19	0.14	0.25	0.51	–
Defibaugh	28	4	18	0.051	−0.017	0.057	0.11	–
de Vries[a]	17	6	139	0.034	−0.025	0.038	0.080	–
Fu	38	4	60	0.057	−0.033	0.057	0.23	–
Fukushima	29	7	57	0.086	−0.13	0.11	0.51	–
Holcomb	31	8	25	0.10	0.057	0.16	0.59	–
Kanungo	39	10	11	0.12	0.38	0.17	0.62	–
Magee	18	6	7	0.041	−0.12	0.055	0.16	–
Malbrunot	32	1, 2	30	0.23	0.032	0.27	0.58	–
Matsuda	5	5	22	0.029	0.033	0.036	0.086	–
Nagel	40	7	27	0.052	0.035	0.063	0.16	–
Qian	41	4	9	0.023	−0.043	0.032	0.095	–
Sato	33	6	21	0.037	−0.035	0.047	0.087	–
Weber[a]	42	3	27	0.033	−0.012	0.039	0.12	–
Weber[a]	43	3	17	0.032	0.049	0.055	0.25	–
Widiatmo	35	5	25	0.35	−0.25	0.50	1.3	–
Zhu	44	4	31	0.23	0.027	0.28	0.56	–

[a] Selected in fitting the ancillary equation.

[b] Methods: (1) manometric, (2) static, (3) glass comparative ebulliometer, (4) Burnett, (5) sinker with magnetic suspension, (6) isochoric with expansion, (7) constant volume, (8) VLE-apparatus, (9) vibrating-tube densimeter, (10) differential manometry.

deviations. Furthermore, the behaviors of thermodynamic surfaces, characteristic curves, and virial coefficients were investigated in these assessments.

The new EOS represents accurately the ideal-gas specific heat as shown in Fig. 2. Data of Yokozeki et al. [7] from 120 to 1000 K can be reproduced with an uncertainty of less than 0.01% even though the upper limit of the EOS is 450 K. Data of Hozumi et al. [23] and Sun et al. [49] are within 0.12 and 0.5%, respectively. The calculated data from the c_p° equation of Sato et al. [27] is within 0.06%.

The reliability assessment for saturation properties derived from the EOS is very important to validate the range of the EOS. The EOS can reproduce reliable vapor pressures with an uncertainty of 0.07% and reliable saturation temperatures with an uncertainty of 0.03 K as shown in Fig. 3. Uncertainties for reliable saturated-liquid and saturated-vapor densities are within 0.2 and 0.7% (at 5 K below the critical point), as shown in Figs. 4 and 5, respectively.

Table VI. Summary of Comparisons for Experimental Data in the Single Phase

Source					AAD	BIAS	STD	Max. Dev.	
First Author	Ref.	Mtd[b]	ϕ[c]	N	(%)	(%)	(%)	(%)	N_{out}
				$p\rho T$ $(y=\rho)$					
Baroncini	36	2	G	93	0.20	0.075	0.24	0.68	4
Bouchot	37	5	L	36	0.077	−0.042	0.090	0.18	–
Bouchot	45	5	L	1433	0.060	−0.024	0.070	0.21	2
Bouchot	45	5	G	622	0.27	−0.057	0.43	3.2	105
Defibaugh	28	3	G	167	0.15	−0.059	0.27	1.7	–
Defibaugh	28	8	L	219	0.16	0.094	0.25	1.8	7
de Vries[a]	17	4	G	565	0.056	−0.011	0.12	0.72	5
de Vries[a]	17	5	L	490	0.11	−0.033	0.25	1.5	8
de Vries	17	2	G	94	0.065	−0.068	0.077	0.24	–
Fu	38	3	G	121	0.19	−0.020	0.25	1.3	–
Fukushima	29	2	G	102	0.53	−0.77	0.86	5.3	6
Fukushima	29	2	L	56	1.0	1.3	1.3	4.1	–
Holste	19	7	L	126	0.14	−0.14	0.22	0.96	–
Magee[a]	18	2	L	137	0.031	0.009	0.037	0.068	–
Malbrunot	32	2	G	86	1.0	−0.96	1.4	4.7	6
Malbrunot	32	1	L	64	0.078	−0.17	0.14	0.83	2
Matsuda[a]	5	9	G	144	0.034	−0.011	0.042	0.12	–
Matsuda[a]	5	9	L	75	0.005	−0.018	0.006	0.029	–
Qian	41	3	G	95	0.081	0.059	0.12	0.72	1
Sato	33	4	G	69	0.17	−0.20	0.26	1.2	5
Takahashi	46	6	G	113	0.31	−0.19	0.55	2.3	3
Zhang	47	3	G	81	0.064	−0.043	0.11	0.81	–
				Speed of sound $(y=w)$					
Grebenkov[a]	22	12	L	30	0.14	0.55	0.19	1.1	–
Grebenkov	48	12	L	93	0.61	1.1	0.67	0.67	2
Hozumi[a]	23	11	G	67	0.006	−0.006	0.007	0.024	–
Pires[a]	16	16	L	305	0.22	0.27	0.36	2.6	2
Sun	49	13	G	38	0.035	0.016	0.046	0.16	–
Takagi[a]	21	10	L	120	0.34	0.30	0.53	3.6	5
				Isobaric specific heat $(y=c_p)$					
Kunimoto	14	14	G	20	0.68	−14	0.95	16	–
Kubota	15	14	G	18	1.0	−14	1.5	17	–
Yomo	50	14	L	19	0.16	−1.1	0.20	1.6	–
				Isochoric specific heat $(y=c_v)$					
Lüddecke[a]	20	15	L	74	0.26	−0.061	0.32	0.85	–

[a] Selected in fitting EOS.

[b] Methods: (1) variable volume, (2) constant volume, (3) Burnett, (4) isochoric with expansion, (5) vibrating-tube densimeter, (6) oscillating-disk viscometer adopted for density measurement, (7) continuously weighed pycnometer, (8) densimeter, (9) sinker with magnetic suspension, (10) echo technique operated at 2 MHz with fixed-path interferometer, (11) spherical acoustic interferometer, (12) impulse method at 2.1 MHz, (13) variable-path acoustic interferometer, (14) flow calorimeter, (15) adiabatic calorimeter, (16) echo technique operated at 1 MHz with fixed-path interferometer.

[c] Grouping of phases according to the original reference, supercritical phase may be included in gaseous phase (G) or liquid phase (L).

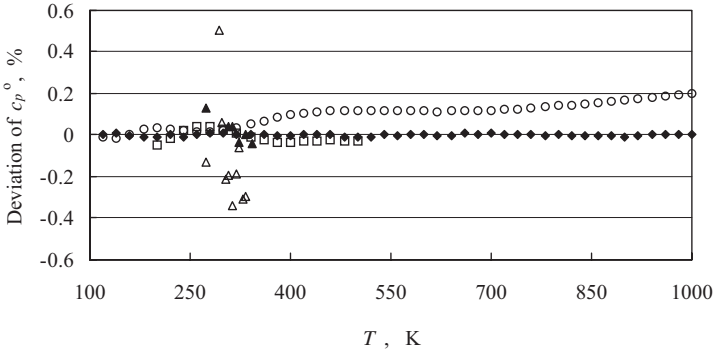

Fig. 2. Deviations of ideal-gas specific heat at constant pressure from the new EOS. (▲) Hozumi et al. [23]; (□) Sato et al. [27]; (△) Sun et al. [49]; (○) Tillner-Roth and Yokozeki [2]; (♦) Yokozeki et al. [7].

Relative deviations in density for the liquid phase are shown in Fig. 6. Very accurate density values can be reproduced. The uncertainties for the data by Matsuda et al. [5] are within 0.01%, data by de Vries [17] within 0.1%, data by Magee [18] within 0.07%, and Defibaugh et al. [28] within 0.5%.

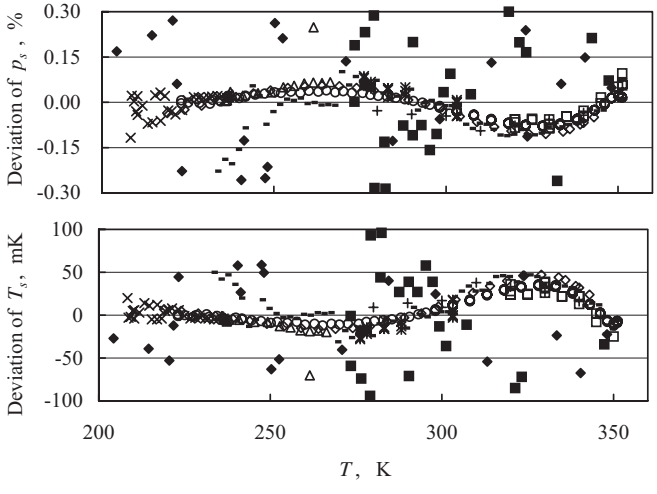

Fig. 3. Deviations of vapor pressures and saturation temperatures from the new EOS. (◇) Defibaugh et al. [28]; (○) de Vries [17]; (–) Fu et al. [38]; (+) Qian et al. [41]; (♦) Malbrunot et al. [32]; (∗) Matsuda et al. [5]; (□) Sato et al. [33]; (×) Weber and Goodwin [42]; (△) Weber and Silva [43]; (■) Zhu et al. [44].

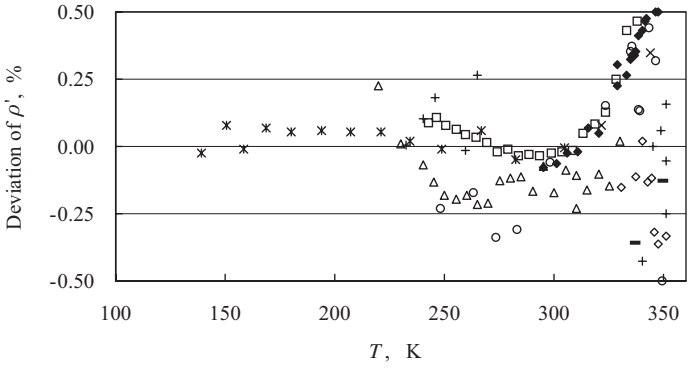

Fig. 4. Deviations of saturated-liquid densities from the new EOS. (□) Defibaugh et al. [28]; (+) Fukushima et al. [29]; (–) Higashi [30]; (♦) Holcomb et al. [31]; (◇) Kuwabara et al. [24]; (∗) Magee [18]; (○) Malbrunot et al. [32]; (×) Sato et al. [33]; (△) Widiatmo et al. [35].

Pressure deviations for superheated-vapor and supercritical phases are shown in Figs. 7 and 8. Deviations in pressure for the superheated-vapor phase are highly accurate compared with the deviations for the supercritical phase. These uncertainties are 0.2 and 0.4% in densities for superheated-vapor and supercritical phases, respectively. Typical uncertainties for the superheated-vapor phase are less than 0.01% in pressure at low densities.

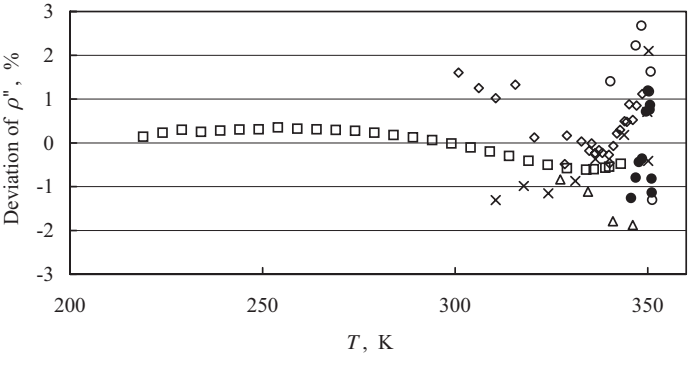

Fig. 5. Deviations of saturated-vapor densities from the new EOS. (□) Defibaugh et al. [28]; (×) Fukushima [29]; (○) Higashi [30]; (◇) Holcomb et al. [31]; (●) Kuwabara et al. [24]; (△) Sato et al. [33].

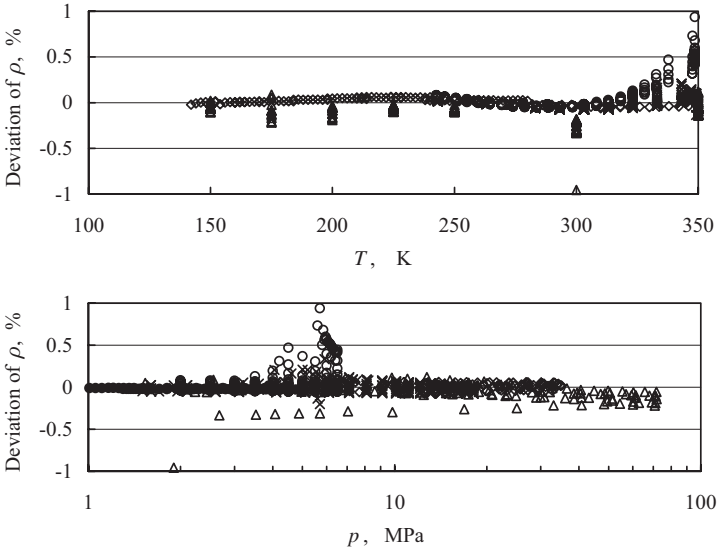

Fig. 6. Deviations of densities in the liquid phase from the new EOS. (○) Defbaugh et al. [28]; (×) de Vries [17]; (◇) Magee [18]; (△) Holste et al. [19].

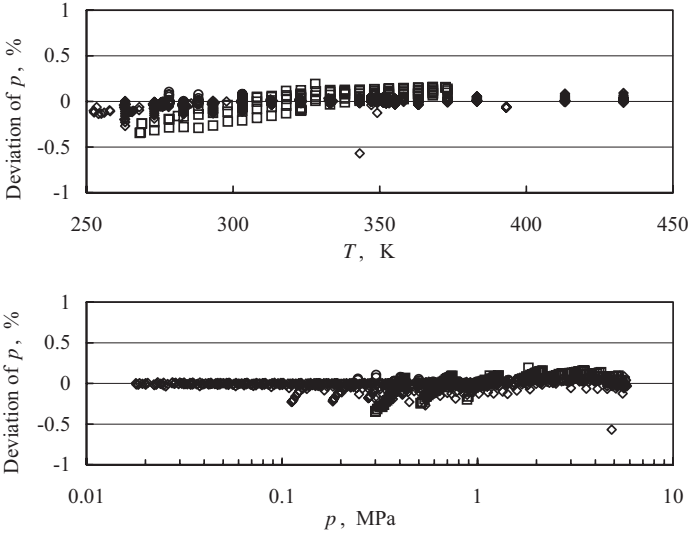

Fig. 7. Deviations of pressures in the superheated-vapor phase from the new EOS. (□) Defibaugh et al. [28]; (△) de Vries [17]; (◇) Matsuda et al. [5].

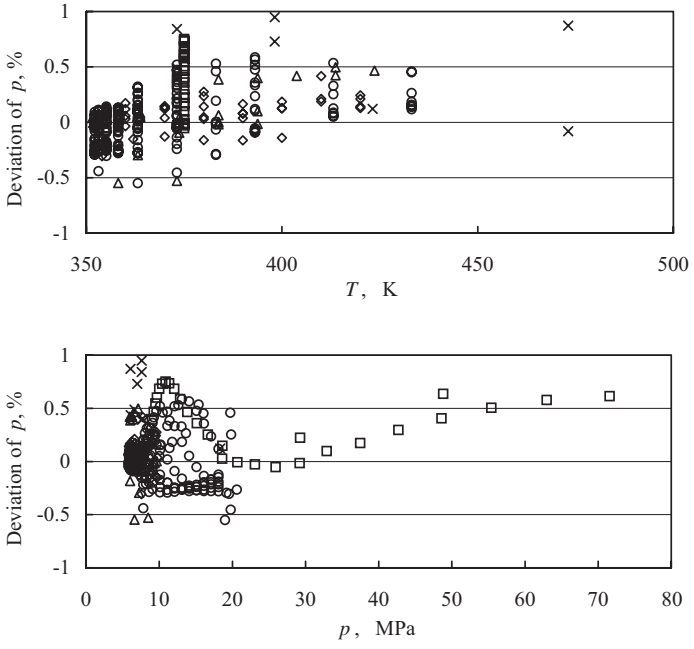

Fig. 8. Deviations of pressures in the supercritical region from the new EOS. (○) de Vries [17]; (△) Fukushima et al. [29]; (□) Holste et al. [19]; (×) Malbrunot et al. [32]; (◇) Sato et al. [33].

The new EOS can accurately reproduce the speed-of-sound data in the gaseous phase, while the accuracy is slightly lower for the liquid phase. For the specific heat, there are three sets of experimental data. The data of Lüddecke and Magee [20] can be reproduced within an uncertainty of 0.6% for c_v in the liquid phase. Although the calculated data for the saturated-liquid specific heat were not fitted by the model, they are reproduced within 0.9% and with an average absolute deviation of less than 0.4%. Yomo et al. [50] reported c_p data in the liquid phase, which are reproduced with deviations of less than 1.5%. Kunimoto et al. [14] reported c_p data in the gaseous phase (the same data as Kubota et al. [15]) which cannot be represented properly. Similar results were also shown by comparing the calculated values from other available EOS. Perhaps the c_p data in the gaseous phase have a highly systematic error. Illustrative results of relative deviations for c_v in the liquid phase, w in the liquid phase, and w in the gaseous phase are given in Figs. 9 to 11, respectively.

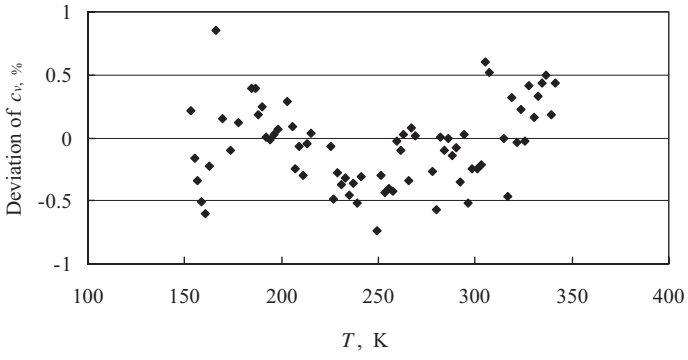

Fig. 9. Deviations of c_v in the liquid phase from the new EOS. (♦) Lüddecke and Magee [20].

Caloric properties can change drastically, approaching either zero or infinity, and it is no longer possible to distinguish gas from liquid at the critical point. Since the Helmholtz EOS is not a theoretical EOS but an empirical one, it should be carefully applied in the critical region. Assessments were conducted by plotting isobaric lines of caloric properties and isothermal lines of $p\rho T$ properties. Figures 12 to 14 show isobaric lines of

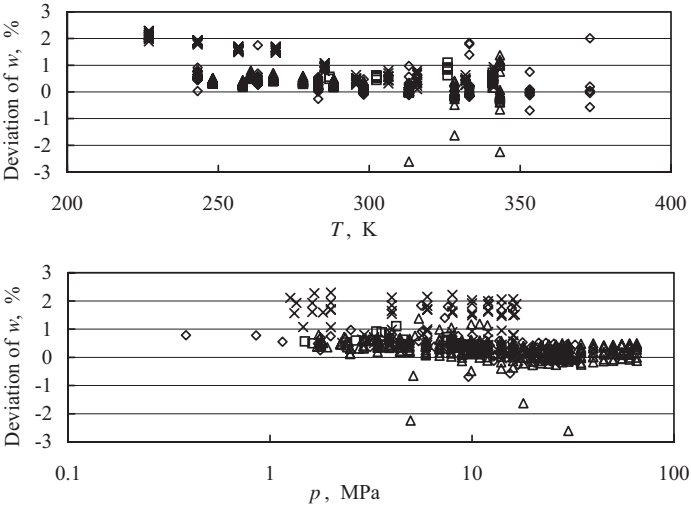

Fig. 10. Deviations of w in the liquid phase from the new EOS. (□) Grebenkov et al. [22]; (×) Grebenkov et al. [48]; (△) Pires and Guedes [16]; (◇) Takagi [21].

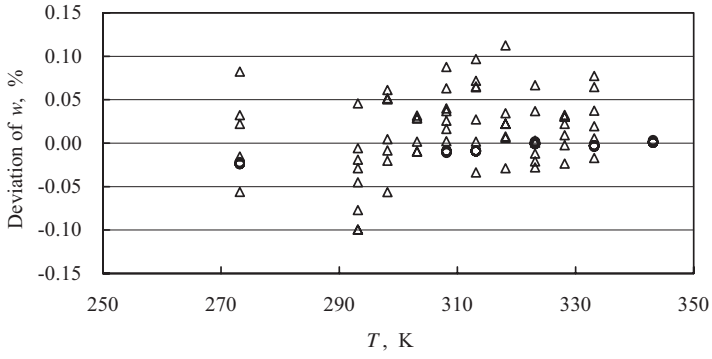

Fig. 11. Deviations of w in the gaseous phase from the new EOS. (○) Hozumi et al. [23]; (△) Sun et al. [49].

the caloric properties for c_p, c_v, and w, respectively, and Fig. 15 shows the p-v-T diagram. As shown in these figures, the new EOS can apparently represent the properties in a wide range of the fluid phase. Using input data as the basis over the range of temperatures up to 423 K and pressures up to 72 MPa, and by considering the reasonable thermodynamic surface of the caloric and $pρT$ properties from a physical viewpoint, the EOS can be safely applied at temperatures from the triple point up to 450 K and pressures up to 72 MPa.

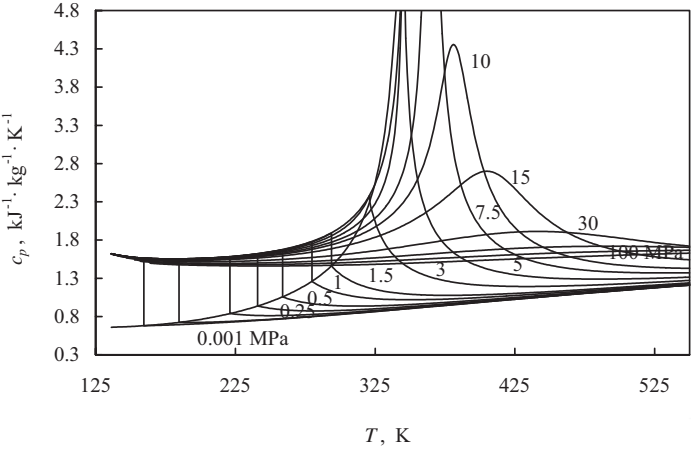

Fig. 12. Isobaric lines of c_p values calculated from the new EOS.

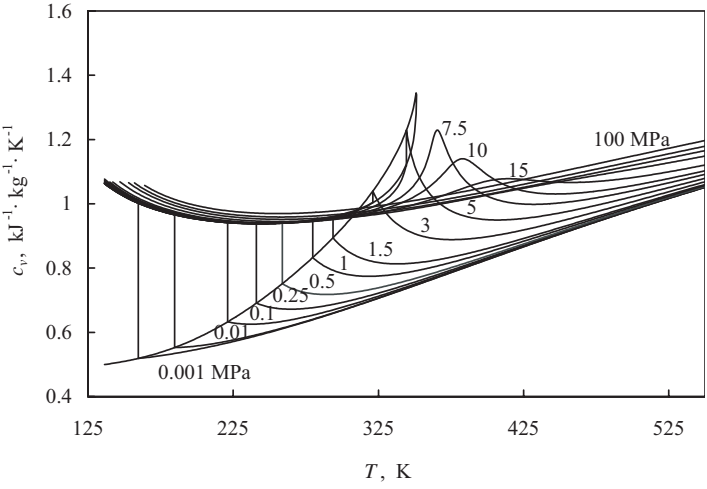

Fig. 13. Isobaric lines of c_v values calculated from the new EOS.

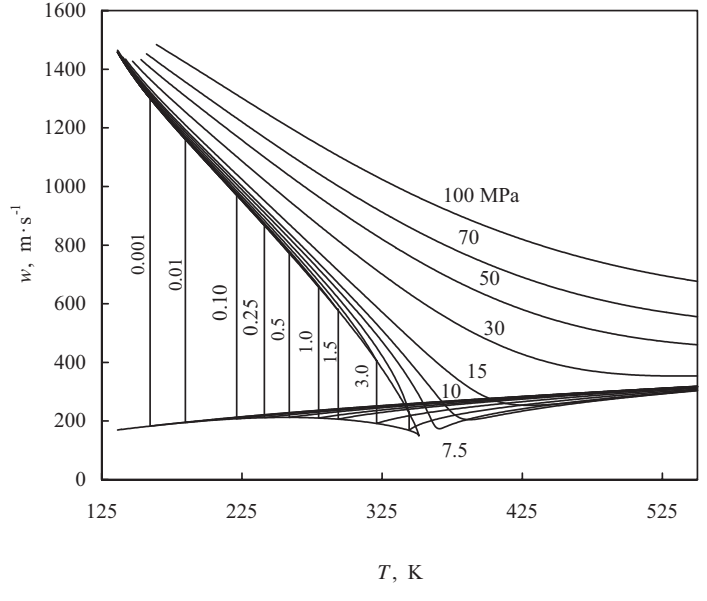

Fig. 14. Isobaric lines of w values calculated from the new EOS.

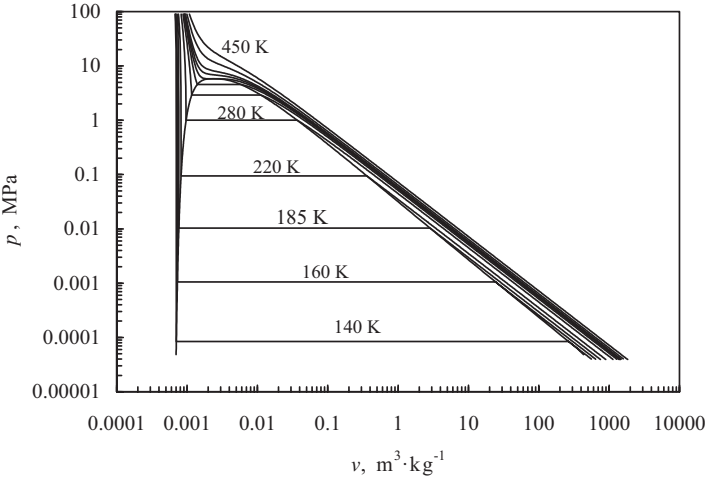

Fig. 15. *p-v-T* diagram calculated from the new EOS.

For caloric properties in the critical region, investigations on isothermal lines of specific heat and speed of sound from the EOS around the critical point are very useful to judge the caloric property behaviors around the critical point and to estimate the caloric properties in the region. Since the new EOS is empirical and data of caloric properties around the critical point are not available, it is not recommended to use the new EOS to estimate caloric properties that are close to the critical region in the range of $|T - T_c| < 3$ K and $|\rho - \rho_c| < 30\ \mathrm{kg \cdot m^{-3}}$.

In principle, the independent critical parameters of the EOS can be obtained by primary and secondary differentiation of pressure with respect to volume in accordance with the critical constraint conditions, i.e., both of the differential values are set to zero. The critical temperature and density were derived from the new EOS by introducing these two constraint conditions, resulting in the values of 351.255 K and 424 $\mathrm{kg \cdot m^{-3}}$ for the critical temperature and density. At these values, the critical pressure is 5.780 MPa. These critical values agree exactly with the critical values selected from the literature [24, 25].

In order to validate the structural form of the EOS and the uncertainties for all thermodynamic properties represented over a wide range of the fluid, characteristic curves of the ideal gas were derived from the EOS. The details of the characteristic curves were given by Span and Wagner [52]. The characteristic curves as shown in Fig. 16 demonstrate that the selection

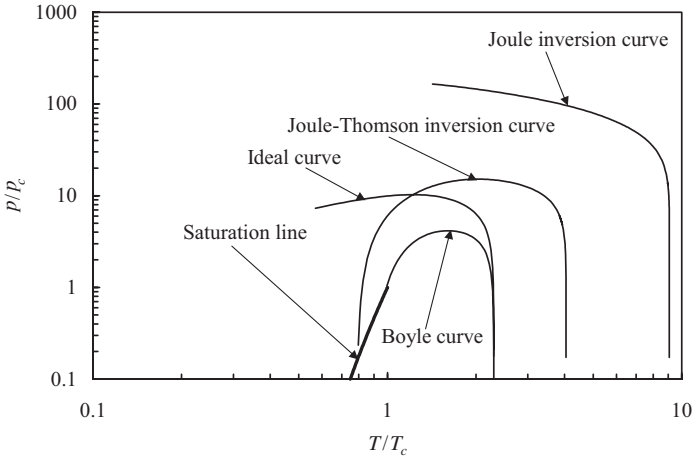

Fig. 16. Characteristic curves calculated from the new EOS.

of the structural form for the EOS is reasonable to represent the thermodynamic properties over a wide range, including the extrapolated range or the range where experimental data are not available.

8. FEATURES OF THE NEW EOS

Improvement of the reliability of the caloric property values calculated from the new EOS in the superheated-vapor phase at low temperatures was the main objective of this study. The consistency of the new EOS with intermolecular potential behavior was investigated with comparisons of second and third virial coefficient values. The results are shown in Figs. 17 and 18. Existing EOS can represent the second virial coefficients reasonably well, but significant differences for the third virial coefficient are indicated especially for the International Standard EOS by Tillner-Roth and Yokozeki [2] and the EOS by Outcalt and McLinden [1] as shown in Fig. 18. A similar shape of the third virial coefficient is observed for the EOS of Outcalt and McLinden, but its values are completely different. On the other hand, the third virial coefficients of the Tillner-Roth and Yokozeki EOS continuously rise to large values as the temperature drops to 0 K. Although the Tillner-Roth and Yokozeki EOS can accurately represent reliable experimental data, the development procedure and input parameters used are not sufficient to ensure the third virial coefficient values to be reliable.

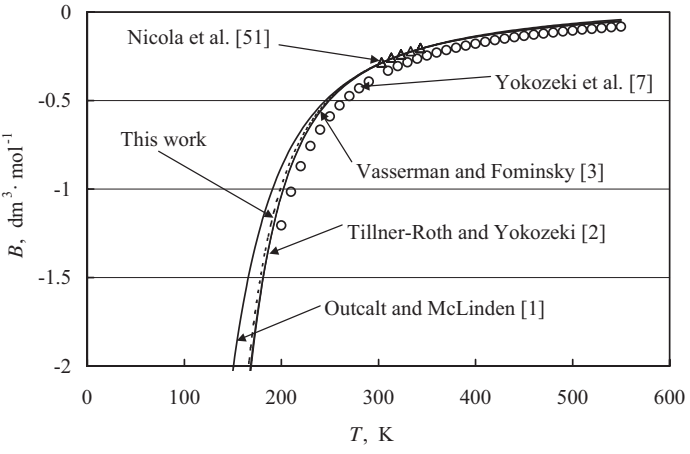

Fig. 17. Comparison of second virial coefficient values.

Values of the specific heat in the gaseous phase at lower temperatures derived from the new EOS were compared with the other EOS. Significantly different c_v values appear near saturation as shown in Fig. 19. Reliable caloric properties in this region are very important for thermodynamic calculation of refrigeration cycles. The new EOS can provide reliable specific heat values that are close to the values based on accurate virial coefficients. Since the virial EOS has a theoretical background, we believe these values are more reliable than those obtained from other empirical EOS based only on experimental data.

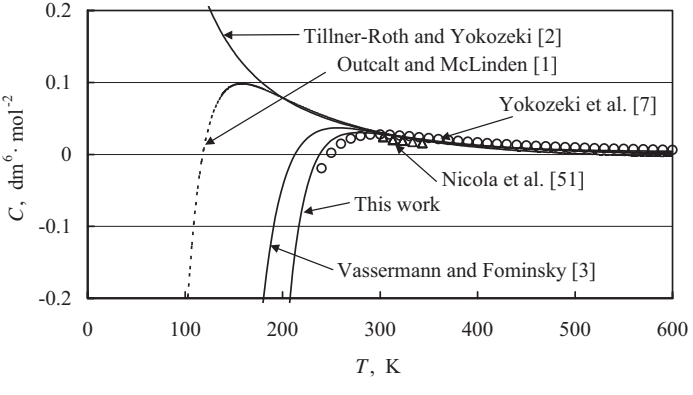

Fig. 18. Comparison of third virial coefficient values.

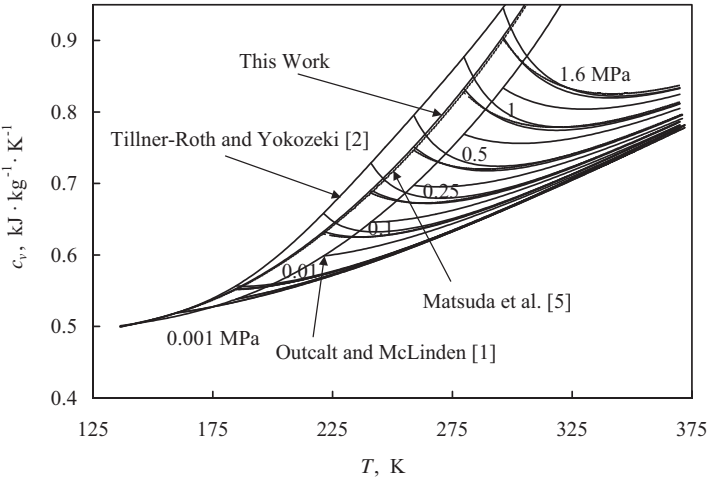

Fig. 19. Comparison of c_v values in the gaseous phase at low temperatures.

9. CONCLUSIONS

A new EOS was established by considering the second and third virial coefficients with a theoretical background. Several sets of the auxiliary data calculated from reliable auxiliary equations were introduced in the development to compensate for the lack of reliable experimental data. Caloric properties in the gaseous phase at low densities were derived from the virial EOS and the equation for the ideal-gas specific heat.

An acceptable accuracy of the new EOS can be achieved by a new method. The intermolecular potential background was included in the method. The new EOS can represent the thermodynamic properties of R32, not only in the region where measured thermodynamic properties are available, but also in the region where experimental data are unavailable. The EOS can provide reliable thermodynamic property values especially in the gaseous phase near saturation and at low temperatures, which is an important range for practical application of air conditioning and refrigeration systems.

The new EOS is valid for temperatures from the triple point to 450 K and at pressures up to 72 MPa. The estimated uncertainties of calculated properties from the EOS are 0.07% in density for the liquid phase, 0.1% in pressure for the gaseous phase, 0.35% in pressure for the supercritical region, 0.07% in vapor pressure, 0.2% in saturated-liquid density, 0.7% in

saturated-vapor density, 0.01% in speed of sound for the gaseous phase, 0.7% in speed of sound for the liquid phase, and 0.6% in isochoric specific heat for the liquid phase.

NOMENCLATURE

a: specific Helmholtz free energy
α: reduced Helmholtz free energy $\alpha = \alpha^o + \alpha^r$, $\alpha = a/RT$
α^o: ideal-gas part of reduced Helmholtz free energy
α^r: residual part of reduced Helmholtz free energy
α^o_τ: primary differential α^o by τ
$\alpha^o_{\tau\tau}$: secondary differential α^o by τ
α^r_τ: primary differential α^r by τ
$\alpha^r_{\tau\tau}$: secondary differential α^r by τ
α^r_δ: primary differential α^r by δ
$\alpha^r_{\delta\delta}$: secondary differential α^r by δ
$\alpha^r_{\delta\tau}$: secondary differential α^r by τ and δ
AAD: average of absolute deviations
BIAS: average of deviations
B: second virial coefficient
C: third virial coefficient
c_p: isobaric specific heat
c^o_p: isobaric specific heat of ideal gas
c_v: isochoric specific heat
c'_s: saturated-liquid specific heat
δ: reduced ρ, ρ/ρ_c,
δ': reduced ρ', ρ'/ρ_c
δ'': reduced ρ'', ρ''/ρ_c
f: fugacity
g: specific Gibbs free energy
h: specific enthalpy
N: number of data
N_i: numerical coefficients of the residual part.
N^o_i: numerical coefficients of the ideal-gas part.
N_{out}: number of rejected data
μ: Joule–Thomson coefficient
p: pressure
p_c: critical pressure
p_s: vapor pressure
φ: phase of fluid
R: gas constant, may be in molar or mass system units, depending on other units in the correlations
ρ: mass density
ρ': saturated-liquid density
ρ'': saturated-vapor density
ρ_c: critical density
s: specific entropy
STD: standard deviation
u: specific internal energy
T: temperature
T_c: critical temperature
τ: inverse reduced temperature, T_c/T
v: specific volume
w: speed of sound
y: evaluated property in deviation
Z: compressibility factor

ACKNOWLEDGMENTS

The authors would like to thank Dr. Eric. W. Lemmon, NIST, for valuable suggestions and discussions in developing the EOS and revising the manuscript.

REFERENCES

1. S. L. Outcalt and M. O. McLinden, *Internat. J. Thermophys.* **16**:79 (1995).
2. R. Tillner-Roth and A. Yokozeki, *J. Phys. Chem. Ref. Data* **26**:1273 (1997).
3. A. A. Vasserman and D. V. Fominsky, *Internat. J. Thermophys.* **22**:1089 (2001).
4. K. Narukawa, A. Mizuoka, and H. Sato, presented at *14th Symp. Thermophys. Props.* (Boulder, Colorado, 2000).
5. N. Matsuda, A. Mizuoka, K. Morita, and H. Sato, *CD-Proc. 16th European Conf. Thermophys. Props, A: Thermophysics of Fluids* (London, 2002).
6. K. A. Gillis and M. R. Moldover, *Internat. J. Thermophys.* **17**:1305 (1996).
7. A. Yokozeki, H. Sato, and K. Watanabe, *Internat. J. Thermophys.* **19**:89 (1998).
8. K. A. Gillis, *Internat. J. Thermophys.* **18**:73 (1997).
9. T. Kojima and H. Sato, *CD-Proc. 16th European Conf. Thermophys. Props. A: Thermophysics of Fluids* (London, 2002).
10. H. L. Zhang, H. Sato, and K. Watanabe, *Proc. 19th Int. Cong. Refrig., IVa* (1995), pp. 622–629.
11. D. B. Fogel, *IEEE Trans. Neural Networks* **5**:3 (1994).
12. I M. Astina and H. Sato, to be submitted to *Internat. J. Thermophys.* (2003).
13. O. Šifner, *Internat. J. Thermophys.* **20**:1653 (1999).
14. Y. Kunimoto, H. Kubota, Y. Tanaka, S. Matsuo, and T. Sotani, *Proc. 15th Japan Symp. Thermophys. Props.* (1994), pp. 149–152.
15. H. Kubota, T. Sonani, and Y. Kunimoto, *Fluid Phase Equilib.* **104**:413 (1995).
16. P. F. Pires and H. J. R. Guedes, *J. Chem. Thermodyn.* **31**:55 (1999).
17. B. de Vries, *DKV-Forsch.-Ber. Nr. 55* (DKV, Stuttgart, 1997).
18. J. W. Magee, *Internat. J. Thermophys.* **17**:803 (1996).
19. J. C. Holste, H. A. Duarte-Garza, and M. A. Villamanan-Olfos, *ASME Winter Annual Meeting* (New Orleans), 93-WA/HT-60 (1993), pp. 1–6.
20. T. O. Lüddecke and J. W. Magee, *Internat. J. Thermophys.* **17**:823 (1996).
21. T. Takagi, *High Temp.-High Press.* **25**:685 (1993).
22. A. J. Grebenkov, O. V. Beljaeva, T. A. Zajatz, and B. D. Timofeev, *Proc. Fourth Asian Thermophys. Props. Conf.* (1995), pp. 311–314.
23. T. Hozumi, H. Sato, and K. Watanabe, *J. Chem. Eng. Data* **39**:493 (1994).
24. S. Kuwabara, H. Aoyama, H. Sato, and K. Watanabe, *J. Chem. Eng. Data* **40**:112 (1995).
25. JARef, *JARef Thermodynamic Tables (in press)*.
26. J. P. Mohr and B. N. Taylor, *J. Phys. Chem. Ref. Data* **28**:1713 (1999).
27. H. Sato, T. Kojima, and K. Ogawa, *Internat. J. Thermophys.* **23**:787 (2002).
28. D. R. Defibaugh, G. Morrison, and L. A. Weber, *J. Chem. Eng. Data* **39**:333 (1994).
29. M. Fukushima, S. Ohotoshi, and T. Miki, *Proc. 19th Internat. Congr. Refrig. IVa* (1995), pp. 207–214.
30. Y. Higashi, *Internat. J. Refrig.* **17**:524 (1994).
31. C. D. Holcomb, V. G. Niesen, L. J. Van Poolen, and S. L. Outcalt, *Fluid Phase Equilib.* **91**:145 (1993).
32. P. F. Malbrunot, P. A. Meunier, G. M. Scatena, W. H. Mears, K. P. Murphy, and J. V. Sinka, *J. Chem. Eng. Data* **13**:16 (1968).
33. T. Sato, H. Sato, and K. Watanabe, *J. Chem. Eng. Data* **39**:851 (1994).
34. K. Shinsaka, N. Gee, and G. R. Freeman, *J. Chem. Thermodyn.* **17**:1111 (1985).
35. J. V. Widiatmo, H. Sato, and K. Watanabe, *J. Chem. Eng. Data* **39**:304 (1994).
36. C. Baroncini, R. Camporese, G. Giuliani, G. Latini, and F. Polonara, *High Temp.-High Press.* **25**:459 (1993).

37. C. Bouchot and D. Richon, *Proc. IIR CFCs, The Day After* (Padova, Italy Comm. B1, B2, E1, E2, 1994), pp. 512–524.
38. Y. D. Fu, L. Z. Han, and M. S. Zhu, *Fluid Phase Equilib.* **111**:273 (1995).
39. A. Kanungo, T. Oi, A. Popowicz, and T. Ishida, *J. Phys. Chem.* **91**:4198 (1987).
40. M. Nagel and K. Bier, *Internat. J. Refrig.* **18**:534 (1995).
41. Z. Y. Qian, A. Nishimura, H. Sato, and K. Watanabe, *JSME Int. J. B.* **36**:665 (1993).
42. L. A. Weber and A. R. H. Goodwin, *J. Chem. Eng. Data* **38:**254 (1993).
43. L. A. Weber and A. M. Silva, *J. Chem. Eng. Data* **39:**808 (1994).
44. M. S. Zhu, J. Li, and B. X. Wang, *Internat. J. Thermophys.* **14:**1221 (1993).
45. C. Bouchot and D. Richon, *Int. Electr. J. Phys.-Chem. Data* **3**:1 (1997).
46. M. Takahashi, N. Shibasaki-Kitakawa, C. Yokoyama, and S. Takahashi, *J. Chem. Eng. Data* **40**:900 (1995).
47. H. L. Zhang, H. Sato, and K. Watanabe, *J. Chem. Eng. Data* **41**:1401 (1996).
48. A. J. Grebenkov, Y. G. Kotelevsky, V. V. Saplitza, O. V. Beljaeva, T. A. Zajatz, and B. D. Timofeev, *Proc. IIR CFCs, The Day After*, Padova, Italy, Comm. B1, B2, E1, E2 (1994), pp. 419–429.
49. L. Q. Sun, Y. Y. Duan, L. Shi, M. S. Zhu, and L. Z. Han, *J. Chem. Eng. Data* **42**:795 (1997).
50. M. Yomo, H. Sato, and K. Watanabe, *High Temp.-High Press.* **26**:267 (1994).
51. G. D. Nicola, F. Polonara, and R. Stryjek, *J. Chem. Eng. Data* **47**:876 (2002).
52. R. Span and W. Wagner, *Internat. J. Thermophys.* **18**:1415 (1997).
53. I M. Astina and H. Sato, *CD-Proc. 16th European Conf. Thermophys. Props. A: Thermophysics of Fluids* (London, 2002).
54. R. Tillner-Roth, *Internat. J. Thermophys.* **17**:1365 (1996).